Chen *et al.*
*Chinese Journal of Mechanical Engineering* (2022) 35:29
https://doi.org/10.1186/s10033-022-00702-7

Chinese Journal of Mechanical Engineering

ORIGINAL ARTICLE

Open Access

# Motion Characteristics Analysis of a Novel Spherical Two-degree-of-freedom Parallel Mechanism

Ziming Chen[1,2*], Xuechan Chen[1,2], Min Gao[1,2], Chen Zhao[1,2], Kun Zhao[1,2] and Yanwen Li[1,2]

**Abstract**

Current research on spherical parallel mechanisms (SPMs) mainly focus on surgical robots, exoskeleton robots, entertainment equipment, and other fields. However, compared with the SPM, the structure types and research contents of the SPM are not abundant enough. In this paper, a novel two-degree-of-freedom (2DOF) SPM with symmetrical structure is proposed and analyzed. First, the models of forward kinematics and inverse kinematics are established based on D-H parameters, and the Jacobian matrix of the mechanism is obtained and verified. Second, the workspace of the mechanism is obtained according to inverse kinematics and link interference conditions. Next, rotational characteristics analysis shows that the end effector can achieve continuous rotation about an axis located in the mid-plane and passing through the rotation center of the mechanism. Moreover, the rotational characteristics of the mechanism are proved, and motion planning is carried out. A numerical example is given to verify the kinematics analysis and motion planning. Finally, some variant mechanisms can be synthesized. This work lays the foundation for the motion control and practical application of this 2DOF SPM.

**Keywords:** Spherical parallel mechanism, 2DOF, Workspace, Equivalent rotation

## 1 Introduction

Spherical parallel mechanism (SPM) is a special spatial parallel mechanism. Its end effector can rotate freely around the point. The SPMs have important application value and have been widely used, such as the azimuth tracking system [1], the bionic robot [2], surgical robot [3], and the medical device [4]. The research about SPM mostly focuses on 2DOF SPM [5] and 3DOF SPM [6]. The theoretical research and practical application of 3DOF SPM are quite mature. For example, theoretical research about the typical 3-RRR 3DOF SPM has been studied in terms of its working space [7], singularity [8], dexterity [9], stiffness [10], dynamics [11]. In practical engineering applications, Gosselin et al. proposed the famous agile eye in 1994 [12], etc. In most cases, the 2DOF SPM can satisfy application requirements, such as pointing mechanisms [13] used in spherical engraving machines, azimuth tracking of satellite antennas, and automatic ground tracking equipment for various aircraft, etc., and some 2DOF artificial wrists sorted out by Bajaj et al. [14].

The representative 2DOF SPM is the spherical 5R mechanism. Ouerfelliz et al. [15] studied the direct and inverse kinematics, kinematic and dynamic optimization of a general spherical 5R linkage. Cervantes-Sanchez et al. [16] analyzed its workspace and singularity. Zhang et al. [17] had a further analysis of the workspace of spherical 5R mechanism and 2DOF SPM with actuation redundancy, as well as dynamic analysis [18, 19], trajectory planning [20], and parameter optimization [21]. Yu et al. [22] introduced a simple and visual graphic method for mobility analysis of parallel mechanisms and presented a novel 2DOF rotational parallel mechanism derived from

*Correspondence: chenzm@ysu.edu.cn
[1] School of Mechanical Engineering, Yanshan University, Qinhuangdao 066004, Hebei, China
Full list of author information is available at the end of the article

well-known Omni Wrist III. Dong et al. [23] analyzed the kinematics, singularity, and workspace of a class of 2DOF rotational parallel manipulators in a geometric approach. Chen [24] proposed a new geometric kinematic modeling approach based on the concept of instantaneous single-rotation-angle and used for the 2DOF RPMs with symmetry in a homo-kinetic plane. Kim et al. [25] deformed the spherical 5R mechanism, designed the spatial self-adaptive finger clamp, and conducted constraint analysis, optimization design of the structure, and grasping experiment on it. Xu et al. [26] established a theory regarding the type synthesis of the two-rotational-degrees-of-freedom parallel mechanism with two continuous rotational axes systematically. Terence et al. [27] conducted the decoupling design of the 5R spherical mechanism and compared it with the traditional 5R spherical mechanism in motion characteristics and workspace. Cao et al. [28] obtained a three-rotation, one-translation (3R1T) manipulator for minimally invasive surgery by connecting the revolute pair and the prismatic pair to a 2DOF spherical mechanism, and analyzed its kinematics and singularity. Alamdar et al. [29] introduced a new non-symmetric 5R-SPM and developed a geometrical approach to analyze its configurations and singularities.

In this paper, a novel 2DOF SPM with symmetric structure and its variant Mechanisms are proposed. The paper is organized as follows: Section 2 gives the description of a SPM structure, analysis of its mobility, the models of forward kinematics and inverse kinematics are established, and the Jacobian matrix of the mechanism is obtained and verified. In Section 3, the workspace of the mechanism is obtained. The rotation characteristics of SMP are analyzed in Section 4. Section 5 describes variant mechanisms of the 2DOF SPM. Conclusions are presented in Section 6.

## 2 Kinematics Analysis of the 2DOF SPM

### 2.1 Mobility Analysis

The schematic diagram of the 2DOF SPM is shown in Figure 1, all the revolute axes intersect at one-point $O$, called the rotation center of the mechanism. The base is connected with the end effector by three spherical serial 3R sub-chains: $B_1B_2B_3$, $B_4B_5B_6$, and $B_7B_8B_9$. There is a special spherical sub-chain consisting of link 9, link 10, and component 11 and connected by two arc prismatic pairs, limiting the revolute axes $OB_2$, $OB_5$, and $OB_8$ on a plane, which is defined as the mid-plane of the mechanism. And the spherical 3R sub-chains $B_7B_8B_9$ and component 11 forming a symmetric double arc slider-rocker mechanism aims at keeping the mid-plane always coplanar with the angular bisector of spherical angle $\angle B_1B_2B_3$ [30], ensuring the base and the end effector are

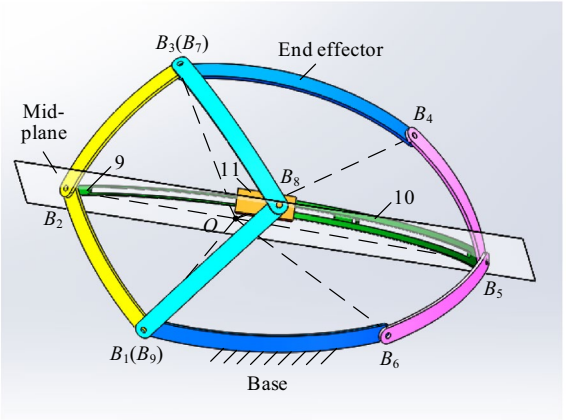


**Figure 1** Schematic diagram of the 2-DOF SPM

symmetric concerning the mid-plane during the movement of the mechanism.

The DOF of the parallel mechanism can be calculated by using the G-K formula:

$$M = d(n - g - 1) + \sum_{i=1}^{g} f_i, \tag{1}$$

where $d$ is the order of a mechanism (for the spherical mechanism $d = 3$), $n$ is the number of components including the base, $g$ is the number of kinematic pairs, $f_i$ is the freedom of the $i$th kinematic pair. For this mechanism $n = 11$, $g = 14$, and $\sum f_i = 14$. Therefore, the degree of freedom of this mechanism is two.

### 2.2 Inverse Kinematics of the SPM

#### *2.2.1 Establishment of the Coordinate Systems*

As shown in Figure 2, a global coordinate system $O$-$x_0y_0z_0$ is located at the rotation center $O$ with the $x_0$-axis passing through point $Q$, the midpoint of arc link $B_1B_2$, the $z_0$-axis is perpendicular to the plane where the arc link $B_1B_2$ lies on, and $y_0$-axis is defined by right-hand rule. The parameter $\theta_{ij}$, where $ij = 21, 32, 43, 54, 65, 61, 74, 87, 81$, represents the angle between the two planes that the two adjacent links lying on. Looking at the rotation center along the revolute axis, the positive direction is counterclockwise.

Due to the characteristics of the SPM that each revolute axis intersects at the rotation center $O$, the parameters $\alpha_i$ and $d_{ij}$ equal zero, where $ij = 21, 32, 43, 54, 65, 61, 74, 87, 81$. The $i$th local coordinate systems are also located at the rotation center $O$. The $x_i$-axis along with each revolute axis, where $x_1$ coincides with $x_9$, $x_2$ coincides with $x_{10}$, $x_3$ coincides with $x_7$, $x_5$ coincides with $x_{11}$, and $x_8$ coincides with $x_{12}$. The $z_i$-axis is perpendicular to

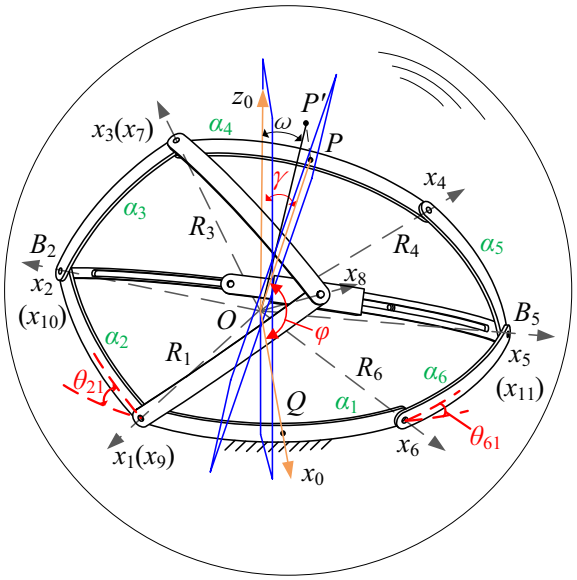


**Figure 2** Kinematic model and parameter representation of the 2-DOF SPM

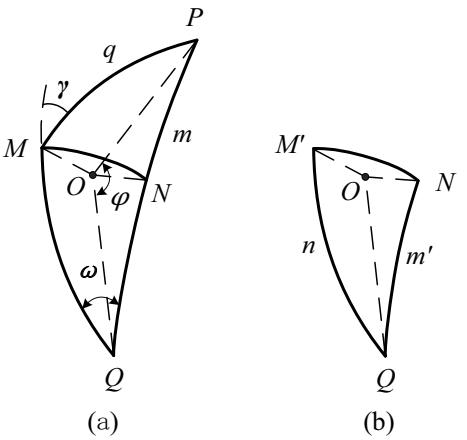


**Figure 3** Schematic of spherical triangle PQM (**a**) and MNQ (**b**)

the plane where the $i$th link is located and the $y_i$-axis is defined by the right-hand rule.

Because this SPM has two DOFs, the configuration can be represented by two angles $\phi$ and $\gamma$, where $\phi$ represents the angle between the ***OP*** and $x_0$-axis, and $\gamma$ represents the angle between the mid-perpendicular plane of the end effector and the plane $O$-$x_0z_0$. Designate point $P$ as the output reference point of the mechanism, and the driving parameters of the mechanism are $\theta_{21}$ and $\theta_{61}$.

In the inverse kinematics, the driving parameters $\theta_{21}$ and $\theta_{61}$ can be solved when the configuration parameters $\phi$ and $\gamma$ of the end effector are given.

#### *2.2.2 Description of the Configuration*

Suppose each link moves on a spherical surface with a radius $R$, and the position of outputs reference point $P$ can be described by angle $\phi$ and $\omega$:

$$P = \begin{bmatrix} x \\ y \\ z \end{bmatrix} = R \begin{bmatrix} \cos\varphi \\ \sin\varphi\sin\omega \\ \sin\varphi\cos\omega \end{bmatrix}, \tag{2}$$

where $\omega$ is the angle between the plane $OPQ$ and the plane $O$-$x_0z_0$, which also represents the angle between the projection of ***OP*** on the plane $O$-$y_0z_0$ and the positive direction of the $z_0$-axis. The relationship between $\gamma$ and $\omega$ can be derived from the spherical triangle $PQM$ and $MNQ$. According to the characteristics of the spherical mechanism and the knowledge of spherical trigonometry [31], the relevant parameters are expressed in Figure 3 for clear observation.

The point $M$ in Figure 3(a) is the intersection point of the arc $MQ$ (intersecting line of the mid-perpendicular plane of the end effector and spherical surface) and arc $MP$ (intersecting line of the plane $O$-$x_0z_0$ and spherical surface), and the point $M'$ in Figure 3(b) is the same point with $M$ for convenient description. The point $N$ is the midpoint of the arc $PQ$ (intersecting line of the plane passing through the two lines $OP$ and $OQ$ and spherical surface), that is, the arc $MN$ is the intersecting line of the midplane and spherical surface.

According to the spherical triangular sine theorem, from the spherical triangle $M'NQ$ shown in Figure 3(b) it can be derived that:

$$\frac{\sin\angle M'}{\sin\angle m'} = \frac{\sin\angle N}{\sin\angle n}. \tag{3}$$

Similarly, it is available in a spherical triangle $PQM$ shown in Figure 3(a):

$$\frac{\sin\angle Q}{\sin\angle q} = \frac{\sin\angle M}{\sin\angle m}. \tag{4}$$

In Eqs. (3) and (4), $\angle M$=180°−$\gamma$, $\angle M'$=$\angle M$/2, $\angle m$=$\phi$, $\angle m'$=$\angle m$/2, $\angle q$=$\angle n$, and $\angle N$=90°.

It can be derived from Eqs. (3) and (4) that:

$$\omega = \arcsin\frac{\sin(180-\gamma)\sin\frac{\varphi}{2}}{\sin\left(\frac{180-\gamma}{2}\right)\sin\varphi}. \tag{5}$$

#### *2.2.3 Solutions of Coordinates with Configuration Parameters*

As shown in Figure 3, the circle where arc $B_2B_5$ is located in the large circle corresponding to the middle plane of the mechanism, so the equation of the circle where arc

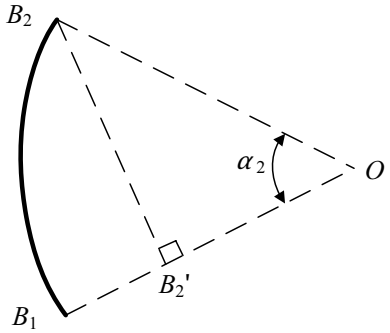


**Figure 4** Front view of link $B_1B_2$

$B_2B_5$ is located in the base coordinate system $O$-$x_0y_0z_0$, can be expressed as

$$\begin{cases} x^2+y^2+z^2=R^2, \\ (\cos\varphi-1)\cdot x+\sin\varphi\sin\omega\cdot y+\sin\varphi\cos\omega\cdot z=0. \end{cases} \tag{6}$$

The trajectory of point $B_2$ in the global coordinate system $O$-$x_0y_0z_0$ is determined by a spherical surface and a plane. As shown in Figure 4, the radius of the spherical surface is $OB_1$ and the center is $O$. The plane is vertical to $\boldsymbol{OB}_1$ and passing through the line $B_2B_2'$.

The trajectory equation is:

$$\begin{cases} x^2+y^2+z^2=R^2, \\ \cos\frac{\alpha_1}{2}\cdot x-\sin\frac{\alpha_1}{2}\cdot y=R\cos\alpha_2. \end{cases} \tag{7}$$

Therefore, the coordinate of $B_2=[x_2\ y_2\ z_2]^{\mathrm{T}}$ in the global coordinate system $O$-$x_0y_0z_0$, can be obtained by Eqs. (6) and (7). And the coordinate of $B_5=[x_5\ y_5\ z_5]^{\mathrm{T}}$ in the global coordinate system $O$-$x_0y_0z_0$, can be obtained similarly.

#### 2.2.4 Solutions of Coordinates with Driving Parameters

The coordinates of $B_2$ and $B_5$ can also be derived by D-H link parameters.

${}_{i}^{i-1}\boldsymbol{T}$ is a forward transformation matrix [32] between the adjacent local $i$th and $(i-1)$th coordinate system, which is the coordinate transformation from $i$th link to $(i-1)$th link, it can be obtained by the following equation:

$${}_{i}^{i-1}\boldsymbol{T}=\mathrm{Rot}(z,\alpha_i)\mathrm{Trans}(0,0,a_i)\mathrm{Trans}(\alpha_{ij},0,0)\mathrm{Rot}(x,\theta_{ij}). \tag{8}$$

${}_{i-1}^{i}\boldsymbol{T}$ is an inverse transformation matrix between the adjacent local $i$th and $(i-1)$th coordinate system, which is the coordinate transformation from $(i-1)$th link to $i$th link, and is the transpose matrix of ${}_{i}^{i-1}\boldsymbol{T}$. Then, it can be derived that:

$${}_{i-1}^{i}\boldsymbol{T}={}_{i}^{i-1}\boldsymbol{T}^{-1}={}_{i}^{i-1}\boldsymbol{T}^{\mathrm{T}}. \tag{9}$$

The coordinates of revolute pairs $B_2$ and $B_5$ in the global coordinate system $O$-$x_0y_0z_0$ can be obtained from Eqs. (8) and (9):

$$\boldsymbol{b_{20}}={}_{0}^{1}\boldsymbol{T}\cdot{}_{1}^{2}\boldsymbol{T}\cdot\boldsymbol{b_{22}}=\begin{bmatrix}x_2\ y_2\ z_2\end{bmatrix}^{\mathrm{T}}, \tag{10}$$

$$\boldsymbol{b_{50}}={}_{0}^{6}\boldsymbol{T}\cdot{}_{6}^{5}\boldsymbol{T}\cdot\boldsymbol{b_{55}}=\begin{bmatrix}x_5\ y_5\ z_5\end{bmatrix}^{\mathrm{T}}, \tag{11}$$

where, $\boldsymbol{b_{55}}=\begin{bmatrix}R\ 0\ 0\end{bmatrix}^{\mathrm{T}}$ are the coordinates of revolute pairs $B_2$ and $B_5$ in the local coordinate system $O$-$x_2y_2z_2$ respectively.

Derived from the coordinate of $\boldsymbol{B}_2=[x_2\ y_2\ z_2]^{\mathrm{T}}$ and Eq. (10):

$$\theta_{21}=\arcsin\frac{z_2}{R\sin\alpha_2}. \tag{12}$$

Derived from the coordinate of $\boldsymbol{B}_5=[x_5\ y_5\ z_5]^{\mathrm{T}}$ and Eq. (11):

$$\theta_{61}=\arcsin\frac{z_5}{R\sin\alpha_6}. \tag{13}$$

In Eqs. (12) and (13), $z_2$ and $z_5$ both have two solutions ($z_2<\pi/2$, $z_2>\pi/2$, $z_5<\pi/2$ and $z_5>\pi/2$), which means one position corresponds to four sets of solutions. The four initial configurations with different arrangements of the drive links are shown in Figure 5.

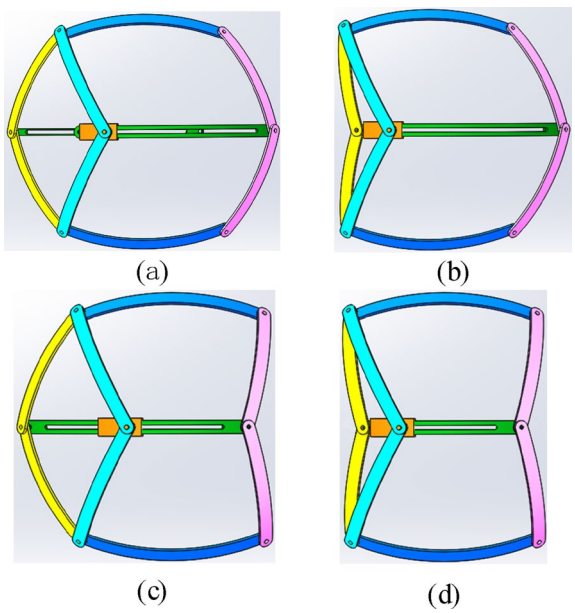


**Figure 5** Four initial configurations with different arrangements of the drive links

Meanwhile, the initial configurations in Figure 5(a) were selected to analyze the kinematics characteristic of the spherical mechanism.

### 2.3 Forward Kinematics of the SPM

Given the driving parameters $\theta_{21}$ and $\theta_{61}$, the solution of the configuration parameters $\phi$ and $\gamma$ can be figured out, that is the forward kinematics of the spherical mechanism. And the normal vector of the mid-plane is obtained by Eqs. (10) and (11):

$$\boldsymbol{b_{20}} \times \boldsymbol{b_{50}} = \begin{bmatrix} r \cdot \boldsymbol{i} & t \cdot \boldsymbol{j} & s \cdot \boldsymbol{k} \end{bmatrix}^{\mathrm{T}}, \tag{14}$$

where,

$$\begin{aligned} r = {} & R^2 \sin\alpha_6 \sin\theta_{61} (\sin\frac{\alpha_1}{2} \cos\alpha_2 + \cos\frac{\alpha_1}{2} \sin\alpha_2 \cos\theta_{21}) \\ & - R^2 \sin\alpha_2 \sin\theta_{21} (\sin\frac{\alpha_1}{2} \cos\alpha_6 + \cos\frac{\alpha_1}{2} \sin\alpha_6 \cos\theta_{61}), \end{aligned}$$

$$\begin{aligned} s = {} & R^2 \sin\alpha_2 \sin\theta_{21} (\cos\frac{\alpha_1}{2} \cos\alpha_6 - \sin\frac{\alpha_1}{2} \sin\alpha_6 \cos\theta_{61}) \\ & - R^2 \sin\alpha_6 \sin\theta_{61} (\cos\frac{\alpha_1}{2} \cos\alpha_2 + \sin\frac{\alpha_1}{2} \sin\alpha_2 \cos\theta_{21}) \\ & - R^2 \sin\alpha_6 \sin\theta_{61} (\cos\frac{\alpha_1}{2} \cos\alpha_2 + \sin\frac{\alpha_1}{2} \sin\alpha_2 \cos\theta_{21}), \end{aligned}$$

$$t = -R^2 (\cos\alpha_6 \sin\alpha_2 \cos\theta_{21} - \cos\alpha_2 \sin\alpha_6 \cos\theta_{61}).$$

The equation of the mid-plane can be described as:

$$r \cdot x + s \cdot y + t \cdot z = 0. \tag{15}$$

The midpoint of the fixed link $Q = [R\ 0\ 0]^{\mathrm{T}}$ and point $P = [x\ y\ z]^{\mathrm{T}}$ are symmetric with respect to the mid-plane. The intersection point of the line $PQ$ and the mid-plane is $H = [x_h\ y_h\ z_h]^{\mathrm{T}}$.

Assuming that $\frac{x_h - R}{r} = \frac{y_h}{s} = \frac{z_h}{t} = k$, the coordinate of the outputs reference point $\boldsymbol{P}$ can be obtained from the symmetrical characteristic of the mechanism:

$$\begin{cases} x = 2x_h - R, \\ y = 2y_h, \\ z = 2z_h. \end{cases} \tag{16}$$

It can be obtained by the spherical triangular cosine theorem from the spherical triangle $M'NQ$ in Figure 3(b) that:

$$\cos\angle M' = -\cos\angle N \cos\angle Q + \sin\angle N \sin\angle Q \cos\angle m'. \tag{17}$$

According to Figure 3(a), the configuration parameters can be obtained by Eqs. (2), (16), and (17):

$$\begin{cases} \varphi = \arccos\frac{x}{R}, \\ \gamma = 180^\circ - 2\arccos(\sin(\arctan\frac{y}{z}) \cos(\frac{1}{2}\arccos\frac{x}{R})). \end{cases} \tag{18}$$

### 2.4 Jacobian Matrix Analysis

By taking the derivative of Eq. (2) with respect to time, the following equation can be obtained:

$$\dot{\boldsymbol{P}} = \begin{bmatrix} \dot{x} \\ \dot{y} \\ \dot{z} \end{bmatrix} = \begin{bmatrix} -R\sin\varphi & 0 \\ R\cos\varphi\sin\omega & R\sin\varphi\cos\omega \\ R\cos\varphi\cos\omega & -R\sin\varphi\sin\omega \end{bmatrix} \begin{bmatrix} \dot{\varphi} \\ \dot{\omega} \end{bmatrix}. \tag{19}$$

From the symmetrical characteristic of the mechanism, we can know that:

$$\begin{cases} \boldsymbol{OB_2} \cdot \boldsymbol{OP} = \boldsymbol{b}_{20} \cdot \boldsymbol{P} = R^2 \cos\angle QOB_2, \\ \boldsymbol{OB_5} \cdot \boldsymbol{OP} = \boldsymbol{b}_{50} \cdot \boldsymbol{P} = R^2 \cos\angle QOB_5. \end{cases} \tag{20}$$

Take the derivative each side of Eq. (20) with respect to time, the following equation can be obtained:

$$\begin{cases} \dot{\boldsymbol{b}}_{20} \cdot \boldsymbol{P} + \boldsymbol{b}_{20} \cdot \dot{\boldsymbol{P}} = R^2 \sin\alpha_2 \sin\frac{\alpha_1}{2} \sin\theta_{21} \cdot \dot{\theta}_{21}, \\ \dot{\boldsymbol{b}}_{50} \cdot \boldsymbol{P} + \boldsymbol{b}_{50} \cdot \dot{\boldsymbol{P}} = R^2 \sin\alpha_6 \sin\frac{\alpha_1}{2} \sin\theta_{61} \cdot \dot{\theta}_{61}, \end{cases} \tag{21}$$

where $\dot{\boldsymbol{b}}_{20} = \begin{bmatrix} \dot{x}_2 & \dot{y}_2 & \dot{z}_2 \end{bmatrix}^{\mathrm{T}}$, $\dot{\boldsymbol{b}}_{50} = \begin{bmatrix} \dot{x}_2 & \dot{y}_2 & \dot{z}_2 \end{bmatrix}^{\mathrm{T}}$.

It can be derived by Eqs. (10), (11), and (19) that:

$$\begin{bmatrix} \dot{\theta}_{21} & \dot{\theta}_{61} \end{bmatrix}^{\mathrm{T}} = \boldsymbol{J} \begin{bmatrix} \dot{\varphi} & \dot{\omega} \end{bmatrix}^{\mathrm{T}}. \tag{22}$$

$\boldsymbol{J}$ in Eq. (22) is the inverse kinematics Jacobian matrix.

$$\boldsymbol{J} = \begin{bmatrix} e_2/d_2 & f_2/d_2 \\ e_6/d_6 & f_6/d_6 \end{bmatrix}, \tag{23}$$

where

$$d_i = D_i(x - R) + E_i y + F_i z,$$

$$e_i = -R(-x_j \sin\varphi + y_j \cos\varphi \sin\omega + z_j \cos\varphi \cos\omega),$$

$$f_i = -R(y_j \sin\varphi \cos\omega - z_j \sin\varphi \sin\omega),$$

$D_i = R\sin\alpha_i \sin\frac{\alpha_1}{2} \sin\theta_{i1}$, $E_i = R\sin\alpha_i \sin\frac{\alpha_1}{2} \cos\theta_{i1}$, $F_i = R\sin\alpha_i \cos\theta_{i1}$, ($i = 2, 6$, when $i = 2$ and 6, $j = 2$ and 5 respectively).

### 2.5 Verification of Kinematic Analysis

When two tiny values are given as inputs, the correctness of the Jacobian matrix and the forward kinematics are verified by comparing the numerical solution of Eqs. (22) and (23) and with the measurements of the 3D model [33].

Four sets of data under two general configurations are given, as shown in Table 1. Then, the correctness of the inverse kinematic model is verified in the same way, which means the correctness of the kinematics analysis of the 2DOF SPM.

## 3 Workspace Analysis

Due to the interference of the mechanism, the reference point $P$ of the end effector can't reach every point on the spherical surface. As shown in Figure 6, suppose the width of each link of the mechanism is 8 mm, the effective radius is $R = 200$ mm, that is, $OP = OQ = 200$ mm, $\alpha_1 = \alpha_4 = 60°$, $\alpha_2 = \alpha_3 = \alpha_5 = \alpha_6 = 40°$, and $\alpha_7 = \alpha_8 = 50°$.

To avoid interference, considering the width of the links, assume that the angle between the rotation axes $OB_1$ and $OB_3$ and the angle between $OB_4$ and $OB_6$ is not less than 10°. The workspace of the mechanism in Figure 6 can be obtained according to the inverse kinematics and the interference condition. The specific limited configuration and corresponding position parameters of the mechanism are shown in Table 2.

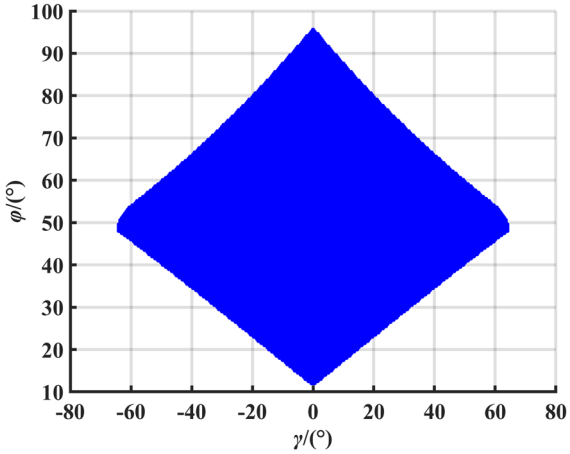


**Figure 6** Workspace of the spherical mechanism

## 4 Equivalent Rotation Characteristics of the Mechanism

### 4.1 Equivalent Rotation Characteristics

The end effector of the 2DOF SPM can realize continuous rotation around the axis that passes through the rotation center and lies on the mid-plane during the moving process. Moreover, the 2DOF SPM also has the following motion properties: Given the initial position and the end position, the end link can realize the pose transformation through a rotation around a fixed axis, which is called the equivalent rotation of the mechanism.

As the simplified motion model shown in Figure 7(a), the end effector moves from position I to position II, and the mid-planes at the initial and final positions are $s_1$ and $s_2$, respectively. The symmetric points of $Q$ about the mid-plane are $P_1$ and $P_2$, respectively. The line $l$ is the intersection line of the two mid-planes, and the axis of

**Table 1** Verification of the Jacobian matrix

| Institutional parameters of the initial configuration (°) | Tiny input $\theta_{21}$, $\theta_{61}$(°) | The theoretical value of Jacques $\varphi$, $\gamma$ ($\times 10^{-3}$ °/s) | The value of the CAD model $\Delta\varphi$, $\Delta\gamma$ ($\times 10^{-3}$ °/s) |
|---|---|---|---|
| $\theta_{21} = 14$ | 0.001 | 3.4397 | 3.4417 |
| $\theta_{61} = 23$ | 0.002 | − 0.3657 | − 0.3505 |
| $\varphi = 59.0786$ | − 0.003 | 0.9701 | 0.8857 |
| $\gamma = -4.7420$ | 0.004 | − 3.6240 | − 3.6368 |
| $\theta_{21} = 31$ | 0.001 | − 1.1911 | − 1.2617 |
| $\theta_{61} = 12$ | − 0.002 | 1.5686 | 1.6108 |
| $\varphi = 64.9472$ | − 0.003 | 1.4643 | 1.6035 |
| $\gamma = 9.2984$ | 0.004 | − 3.5059 | − 3.5913 |

**Table 2** Limited configuration parameters of the spherical mechanism

| Limited configuration | $\varphi$ (°) | $\lambda$ (°) | Configuration of the mechanism |
|---|---|---|---|
| 1 | 49.8502 | − 67.5085 | 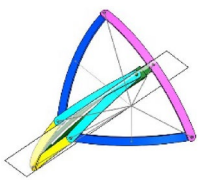 |
| 2 | 49.8502 | 67.5085 | 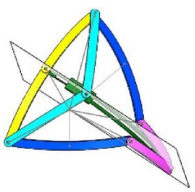 |
| 3 | 95.8430 | 0 | 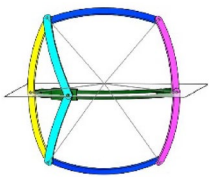 |
| 4 | 11.5519 | 0 |  |

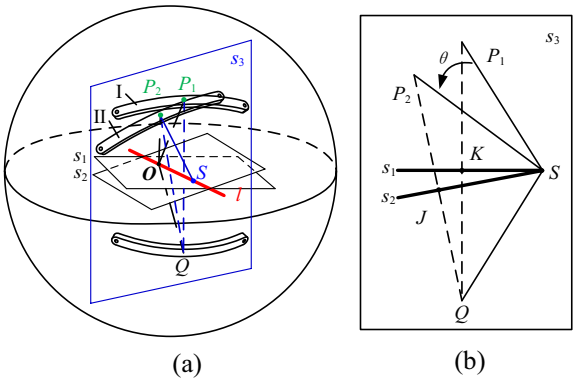


**Figure 7** Schematic diagram of the initial and final configuration (**a**) and front view of plane $s_3$ (**b**)

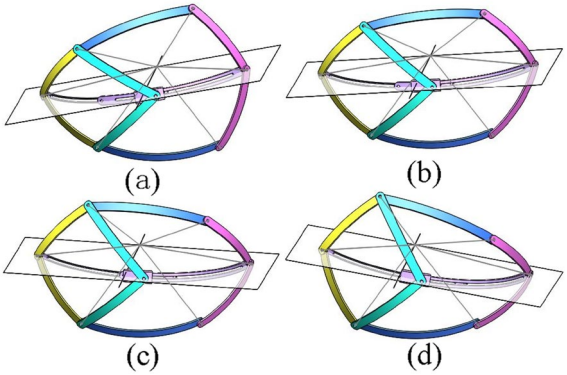


**Figure 8** Numerical example of the equivalent rotation

the equivalent rotation [34]. For a clear obversion, a plane $s_3$ is set, which passes through line $OP_1$ and is perpendicular to line $l$, as shown in Figure 7(b). $S$ is the intersection point of the line $l$ and the plane $s_3$. $K$ is the intersection point of line $QP_1$ and plane $s_1$. $J$ is the intersection point of line $QP_2$ and plane $s_2$.

### 4.2 How to Realize the Equivalent Rotation

As shown in Figure 7(a), the two parameters $\phi_1$ and $\gamma_1$ of the initial configuration of the mechanism and the two parameters $\phi_2$ and $\gamma_2$ of the final configuration are given. The coordinates of output reference point can be obtained by Eq. (2). The equation of axis $l$, which is the intersection line of the two mid-planes, can be obtained by Eq. (15). The equation of plane $s_3$, which is passing through lines $QP_1$ and $QP_2$, can be obtained according to the structural characteristics. And the coordinates of the point $S$ can be obtained by the equations of axis $l$ and plane $s_3$.

Then the rotated angle of the output reference point $P$ can be derived that:

$$\theta = \arccos\left(\frac{\boldsymbol{SP_1}\cdot\boldsymbol{SP_2}}{|\boldsymbol{SP_1}|\cdot|\boldsymbol{SP_2}|}\right), \tag{24}$$

where $\boldsymbol{SP_1} = \boldsymbol{P_1} - \boldsymbol{S}$ and $\boldsymbol{SP_2} = \boldsymbol{P_2} - \boldsymbol{S}$.

The direction vector $\boldsymbol{l} = [l_x\ l_y\ l_z]^{\mathrm{T}}$ and the rotation angle $\theta$ of the end effector rotating around the axis $l$ are already obtained, and the rotation matrix $\boldsymbol{R}_{(\theta)}$ can be expressed by:

$$\boldsymbol{R}_{(\theta)} = \begin{bmatrix} l_x l_x\xi + \cos\theta & l_y l_x\xi - l_z\sin\theta & l_z l_x\xi + l_y\sin\theta \\ l_x l_y\xi + l_z\sin\theta & l_y l_y\xi + \cos\theta & l_z l_y\xi - l_x\sin\theta \\ l_x l_z\xi - l_y\sin\theta & l_y l_z\xi + l_x\sin\theta & l_z l_z\xi + \cos\theta \end{bmatrix}, \tag{25}$$

where $\xi = (1 - \cos\theta)$.

The vector $\boldsymbol{QP_2}$ can be expressed as:

$$\boldsymbol{QP_2} = \boldsymbol{R}_{(\theta)}\boldsymbol{SP_1} + \boldsymbol{QS}. \tag{26}$$

The coordinates of point $P_2$ can be obtained by Eq. (26), and the other parameters of the mechanism can be obtained by the inverse kinematics described in Section 2.2. Thereby, the driving parameters $\theta_{21}$ and $\theta_{61}$ of the rotation process can be obtained. It provides the basis for the motion planning of the spherical mechanism.

### 4.3 Motion Planning of the Equivalent Rotation

As shown in Figure 2, suppose the effective radius is $R = 200$ mm, that is, $OP = OQ = 200$ mm, $\alpha_1 = \alpha_4 = 60°$, $\alpha_2 = \alpha_3 = \alpha_5 = \alpha_6 = 40°$, and $\alpha_7 = \alpha_8 = 50°$. The parameters of the initial position are $\phi_1 = 75°$, $\gamma_1 = -20°$, and the parameters of final position are $\phi_2 = 70°$, $\gamma_2 = 20°$. The four configurations of the mechanism from the initial position to the final position are shown in Figure 8(a)–(d), respectively. The detailed parameters of each configuration are listed in Table 3.

## 5 Variant Mechanisms of the 2DOF SPM

Based on the 3DOF planar sub-chain, a group of variant 2DOF SPMs with the same characteristics are synthesized, providing more potential possibilities for practical application.

In the middle of this mechanism, there are two arc prismatic pairs connecting links 9, 10, and 11, which function to keep the lines $OB_2$, $OB_5$, and $OB_8$ on the same mid-plane. According to the mechanism theory, the 3DOF planar sub-chain can restrict the revolute to the middle plane of the mechanism, ensuring that the relative motion between each motion pair is only planar. Therefore, the 3DOF planar sub-chains are used to replace the spherical links to provide the same constraints. By this method, a set of 2DOF SPMs without arc prismatic pairs can be obtained.

**Table 3** Numerical calculation example of the equivalent rotation

| | **Configuration 1 ($\theta = 0°$)** | **Configuration 2 ($\theta = 13°$)** | **Configuration 3 ($\theta = 26°$)** | **Configuration 4 ($\theta = 40°$)** |
|---|---|---|---|---|
| Equation of rotation axis | $\frac{x}{-0.7933} = \frac{y}{0.1257} = \frac{z}{-0.5957}$ | | | |
| Institutional configuration $\varphi, \gamma$ | $\varphi = 75°$<br>$\gamma = -20°$ | $\varphi = 74.5°$<br>$\gamma = -7.1°$ | $\varphi = 72.9°$<br>$\gamma = -5.8°$ | $\varphi = 70°$<br>$\gamma = 20°$ |
| Driving angle | $\theta_{21} = 5.3°$<br>$\theta_{61} = 56.7°$ | $\theta_{21} = 18.3°$<br>$\theta_{61} = 35.3°$ | $\theta_{21} = 32.3°$<br>$\theta_{61} = 18.9°$ | $\theta_{21} = 49.2°$<br>$\theta_{61} = 3.7°$ |

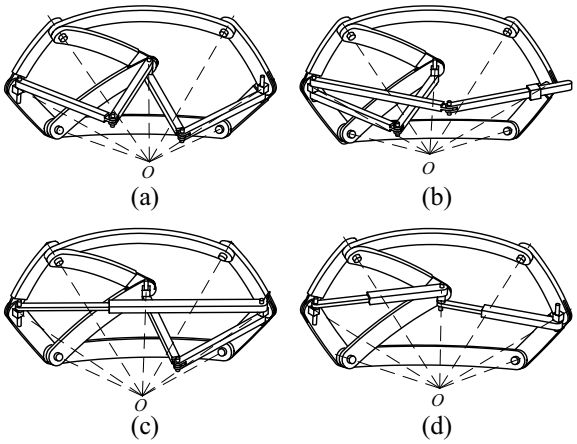


**Figure 9** Several 2DOF SPMs based on 3DOF planar sub-chain

There are seven different configurations of the 3DOF planar sub-chain can be obtained: [RRR], [RPR], [PRR], [RRP], [PPR], [PRP], [RPP], in which *R* represents revolute pair and *P* represents prismatic pair [34]. Based on the 3DOF constrained planar sub-chain, seven kinds of equivalent 2DOF SPMs can be obtained, four of which are shown in Figure 9.

## 6 Conclusions

A novel 2DOF Spherical Parallel Mechanism (SPM) is proposed. The SPM can realize continuous rotation around any line on the mid-plane which passes through the rotation center of the spherical mechanism, and the rotational axis can be fixed during the rotation process, which means any form of motion of the mechanism can be transformed into a rotation with a fixed axis.

The forward and inverse kinematics of the mechanism are solved based on D-H parameters and analytical geometry. The inverse Jacobian matrix of the 2DOF SPM is obtained by taking the derivative of the constraint equation, and its workspace is analyzed by considering the interference condition of the links. The correctness of the kinematics and motion planning of the mechanism is verified by the motion examples presented.

A group of variant 2DOF SPMs are constructed based on the different 3DOF planar sub-chain that can provide more possibilities for practical application.

**Acknowledgements**
The authors sincerely thanks to Professor Zhen Huang of Yanshan University for his critical discussion and reading during manuscript preparation.

**Authors' contributions**
ZC was in charge of the whole trial; XC wrote the manuscript; MG, CZ, KZ and YL assisted with sampling and laboratory analyses. All authors read and approved the final manuscript.

**Authors' information**
Ziming Chen, born in 1984, is currently an associate professor at *Yanshan University, China*. He received his Ph.D. degree from *Yanshan University, China*. His research interests include the design and analysis theory of parallel mechanism, robot technology. E-mail: chenzm@ysu.edu.cn
Xuechan Chen, born in 1995, is currently a PhD candidate at *the School of Mechanical Engineering, Yanshan University, China*. Her research interests include parallel mechanism. E-mail: chenxc@stumail.ysu.edu.cn
Min Gao, born in 1994. She received her master degree from *Yanshan University, China,* in 2020.
Chen Zhao, born in 1992, is currently a PhD candidate at *School of Mechanical Engineering, Yanshan University, China*. He received his master degree from *Yanshan University, China*, in 2017. His research interests include parallel robot and parallel machine tool. E-mail: zchen@stumail.ysu.edu.cn
Kun Zhao, born in 1997, is currently a master candidate at *the School of Mechanical Engineering, Yanshan University, China*. E-mail: zhaok@stumail.ysu.edu.cn
Yanwen Li, born in 1966, is currently a professor at *Yanshan University, China*. She received her Ph.D. degree from *Yanshan University, China*. E-mail: ywl@ysu.edu.cn

**Funding**
Supported by National Natural Science Foundation of China (Grant No. 51775474)

**Competing interests**
The authors declare no competing financial interests.

**Author Details**
[1]School of Mechanical Engineering, Yanshan University, Qinhuangdao 066004, Hebei, China. [2]Parallel Robot and Mechatronic System Laboratory of Hebei Province, Yanshan University, Qinhuangdao 066004, Hebei, China.

Received: 19 February 2021 Revised: 9 February 2022 Accepted: 10 March 2022
Published online: 05 April 2022

**References**

[1] J Luo, H Liu, S Yu, et al. Development of an image-based visual servoing for moving target tracking based on bionic spherical parallel mechanism.

*Proceedings of the 2014 IEEE International Conference on Robotics and Biomimetics,* Bali Indonesia: IEEE, 2014: 1633-1638.
[2] S Kumar, B Bongardt, M Simnofske, et al. Design and kinematic analysis of the novel almost spherical parallel mechanism active ankle. *Journal of Intelligent & Robotic Systems*, 2019, 94(2): 303-325.
[3] D Chablat, G Michel, P, Bordure, et al. Workspace analysis in the design parameter space of a 2-DOF spherical parallel mechanism for a prescribed workspace: application to the otologic surgery. *Mechanism and Machine Theory*, 2021: 157.
[4] H Saafi, M A Laribi, S Zeghloul. Optimal torque distribution for a redundant 3-RRR spherical parallel manipulator used as a haptic medical device. *Robotics and Autonomous Systems*, 2017, 89: 40-50.
[5] B Bian, L Wang. Design, analysis, and test of a novel 2-DOF spherical motion mechanism. *IEEE Access*, 2020, 8: 53561-53574.
[6] J A Leal Naranjo, M Wang, J C Paredes Rojas, et al. Design and kinematic analysis of a new 3-DOF spherical parallel manipulator for a prosthetic wrist. *Journal of the Brazilian Society of Mechanical Sciences and Engineering*, 2020, 42: 63.
[7] S Bai. Optimum design of spherical parallel manipulators for a prescribed workspace. *Mechanism and Machine Theory*, 2010, 45(2): 200–211.
[8] I Bonev, C Gosselin. Singularity loci of spherical parallel mechanisms. *IEEE International Conference on Robotics & Automation,* 2005: 2957–2962.
[9] C Gosselin, J Angeles. A Global Performance index for the kinematic optimization of robotic manipulators. *ASME Journal of Mechanical Design*, 1991, 113: 220-226.
[10] C Gosselin. Stiffness mapping for parallel manipulators. *IEEE Transactions on Robotics and Automation,* 1990, 6(3): 377-382.
[11] B Danaei, A Arian, M T Masouleh, et al. Dynamic modeling and base inertial parameters determination of a 2-DOF spherical parallel mechanism. *Multibody System Dynamics*, 2017, 41(4): 367–390.
[12] C Gosselin, J F Hamel. The agile eye: a high-performance three-degree-of-freedom camera-orienting device. *IEEE International Conference on Robotics & Automation,* IEEE, 1994: 781–786.
[13] J Yu, K Wu, G Zong, et al. A comparative study on motion characteristics of three two-degree-of-freedom pointing mechanisms. *Journal of Mechanisms and Robotics-Transactions of the ASME,* 2016, 8(2): 021027.
[14] N M Bajaj, A J Spiers, A M Dollar. State of the art in artificial wrists: a review of prosthetic and robotic wrist design. *IEEE Transactions on Robotics*, 2019, 35 (1): 261-277.
[15] M Ouerfelli, V Kumar. Optimization of a spherical five-bar parallel drive linkage. *Trans.of the ASME J.of Mechanical Design*, 1994, 116(1): 166–173.
[16] J J Cervantes Sanchez, J C Hernandez Rodriguez, E J Gonzalez-Galvan. On the 5R spherical, symmetric manipulator: workspace and singularity characterization. *Mechanism and Machine Theory*, 2004, 39(4): 409-429.
[17] L J Zhang, Y W Niu, Y Q Li, et al. Analysis of the workspace of 2-DOF spherical 5R parallel manipulator. 2006 *IEEE International Conference on Robotics and Automation*, 2006: 1123-1128.
[18] Y Li, L Zhang, Y Niu. Dynamic analysis of spherical 2-DOF parallel manipulator with actuation redundancy. *2011 IEEE International Conference on Mechatronics and Automation,* Beijing, China, IEEE, 2011.
[19] L J Zhang, Y Q Li, Y Q Guo. Dynamic analysis of spherical 5R Parallel Manipulator. *International Conference on Mechatronics & Automation*, 2009.
[20] Y Q Li, Y W Niu. Dynamic analysis of spherical 2-DOF parallel manipulator with actuation redundancy. *2011 IEEE Int. Conf. Mech. Autom*, 2011: 1350-1355.
[21] L J Zhang, Y Q Li, W Y Shi. Parameter optimum design of spherical 2-DOF parallel manipulator with actuation redundancy. *2009 International Conference on Mechatronics and Automation*. IEEE, 2009.
[22] J J Yu, X Dong, X Pei, et al. Mobility and singularity analysis of a class of 2-DOF rotational parallel mechanisms using a visual graphic approach. *Asme International Design Engineering Technical Conferences & Computers & Information in Engineering Conference*, 2011.
[23] X Dong, J Yu, B Chen, et al. Geometric approach for kinematic analysis of a class of 2-DOF rotational parallel manipulators. *Chinese Journal of Mechanical Engineering*, 2012, 25(2): 241–247.
[24] B Chen . Dynamic modeling and analysis of 2-DOF quasi-sphere parallel platform. *Journal of Mechanical Engineering*, 2013, 49(13): 24.
[25] Y Xu, D Zhang, M Wang, et al. Type synthesis of two-degrees-of-freedom rotational parallel mechanism with two continuous rotational axes. *Chinese Journal of Mechanical Engineering*, 2016, 29 (4): 694-702.
[26] K Tae Uk, O Yonghwan. IEEE: Design of spatial adaptive fingered gripper using spherical five-bar mechanism. *2014 International Conference on Advanced Mechatronic Systems*, 2014: 145-150.
[27] Essomba, Terence, Linh, et al. Kinematic analysis of a new five-bar spherical decoupled mechanism with two-degrees of freedom remote center of motion. *Mechanism & Machine Theory Dynamics of Machine Systems Gears & Power Trandmissions Robots & Manipulator Systems Computer Aided Design Methods*, 2018.
[28] W A Cao, S J Xu, K Rao, et al. Kinematic design of a novel two degree-of-freedom parallel mechanism for minimally invasive surgery. *Journal of Mechanical Design*, 2019, 141(10): 104501.
[29] A Alamdar, F Farahmand, S Behzadipour, et al. A geometrical approach for configuration and singularity analysis of a new non-symmetric 2DOF 5R spherical parallel manipulator. *Mechanism and Machine Theory*, 2020, 147: 103747.
[30] W Ding, Y A Yao. Self-crossing motion analysis of a novel inpipe parallel robot with two foldable platforms. *Transmissions and Applications*, 2015: 221-229.
[31] J B Shor. Kinematics of spherical mechanisms. *Cambridge University Press*, 1988.
[32] J J Craig. Introduction to robotics: mechanics and control. *Pearson Education*, Inc, 1986.
[33] E Cuan Urquizo, E Rodriguez Leal. Kinematic analysis of the 3-CUP parallel mechanism. *Robotics and Computer-Integrated Manufacturing*, 2013, 29(5): 382-395.
[34] Z Chen, W A Cao, Z Huang. Type synthesis of 3-DOF rotational parallel mechanisms with no intersecting axes. *ASME International Design Engineering Technical Conferences & Computers & Information in Engineering Conference*, 2012.